Inorganic Chemistry

Article

pubs.acs.org/IC

Syntheses and Magnetic Properties of New Tellurite–Sulfate Compounds $M_2(TeO_3)(SO_4)\cdot H_2O$ (M = Co, Mn) with a Layer Structure Showing a Distorted Honeycomb Spin–Lattice

Yingying Tang,[†,‡] Zhangzhen He,*[,†] Wenbin Guo,[†] Suyun Zhang,[†] and Ming Yang[†]

[†]State Key Laboratory of Structural Chemistry, Fujian Institute of Research on the Structure of Matter, Chinese Academy of Sciences, Fuzhou, Fujian 350002, P. R. China

[‡]Graduate School of the Chinese Academy of Sciences, Beijing 100039, P. R. China

Supporting Information

ABSTRACT: New tellurite–sulfate compounds $M_2(TeO_3)(SO_4)\cdot H_2O$ (M = Co, Mn) are synthesized by a conventional hydrothermal method. Two compounds are found to exhibit a similar structure, which both crystallize in the orthorhombic system of space group *Pbcm*. Te^{4+} ions are coordinated by three O atoms, forming a quite distorted TeO_3 trigonal pyramid with lone-pair electrons, while magnetic Co^{2+} or Mn^{2+} ions construct a wavelike layer with a distorted honeycomb spin–lattice. Magnetic measurements confirm that two isostructural compounds display different magnetic behaviors, in which $Co_2(TeO_3)(SO_4)\cdot H_2O$ shows a canted antiferromagnetic ordering at ~15 K, while $Mn_2(TeO_3)(SO_4)\cdot H_2O$ shows a collinear antiferromagnetic ordering at ~28 K. The nature of different magnetic behaviors between two isostructural compounds is also discussed.

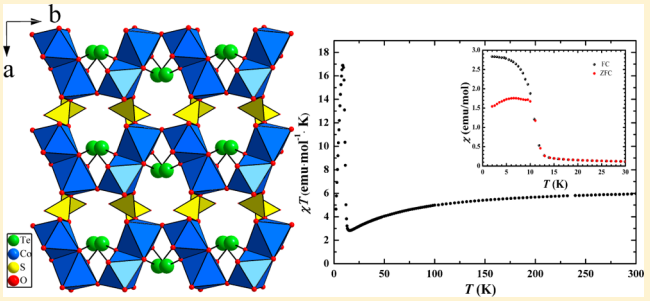

INTRODUCTION

The search for 3d transition-metal oxides with a two-dimensional (2D) layer structure has attracted great interest in the scientific community in the last decades since the discovery of high-T_c CuO-based superconductors. With an intensive study, many 2D compounds have been constructed and synthesized that are found to display various interesting structural features with a unique spin–lattice such as square planar, triangle, or honeycomb. Usually 2D compounds with a unique spin–lattice can be found to exhibit distinct electronic configurations and unusual magnetic properties. For example, the Wigner crystallization of magnons is realized in 2D orthogonal spin-dimer compound $SrCu_2(BO_3)_2$ with a square-planar lattice,[1] while the Bose–Einstein condensation of magnons is observed in 2D bilayer system $BaCuSi_2O_6$.[2] Jarosite $KFe_3(SO_4)_2(OH)_6$ is considered as a typical kagomé lattice that shows a spin-frustration effect,[3] while $Bi_3Mn_4O_{12}(NO_3)$ with a honeycomb lattice is found to show a spin liquid ground state.[4] Such a correlation of the magnetic properties and structural features has been a hot topic in the fields of chemistry and physics, which accelerates continuously the exploration of new 2D compounds with new magnetic phenomena.

It is well-known that the magnetic properties of compounds are mainly determined by the arrangements of the magnetic ions in the geometrical topology. However, spin–lattices constructed by magnetic ions are also affected strongly by nonmagnetic subgroups in the structural framework. A typical example is the 2D spin-dimer compound $SrCu_2(BO_3)_2$ mentioned above, in which Cu_2O_6 dimers are linked orthogonally via BO_3 subgroups, forming a square-planar network in a layer.[5] Such a structural feature cannot been seen in similar compounds such as $BaCu_2Si_2O_7$,[6] $SrCu_2(PO_4)_2$,[7] or $BaCu_2V_2O_8$,[8] of which compounds belong to the family formulated as $ACu_2X_2O_n$ (A = Ba, Pb, Sr; X = B, Si, Ge, P, V; *n* = 6, 7, 8). This indicates that nonmagnetic subgroups would play an important role in the construction of structural frameworks, even for spin–lattices related to magnetic ions.

To explore new transition-metal-based oxides and to further investigate interesting magnetic phenomena, our current motivation is focused on selecting the known compounds as models and further designing new compounds through a partial substitution of subgroups such as SO_4^{2-}, TeO_4^{2-}, BO_3^{3-}, PO_4^{3-}, SiO_4^{4-}, GeO_4^{4-}, and so on. On the basis of this idea, we have synthesized a new compound, $SrCo_2BPO_7$,[9] showing interesting magnetic behaviors through the partial substitution of BO_3^{3-} for PO_4^{3-} of $SrCo_2(PO_4)_2$. In our recent study, we try to find new tellurite–sulfate compounds by selecting transition-metal sulfates as model compounds with the partial substitution of TeO_4^{2-} for SO_4^{2-}. It must be noted that 3d transition-metal tellurite–sulfate compounds are rarely reported previously. Up to now, only a few natural minerals and prepared compounds such as Poughite $Fe_2SO_4(TeO_3)\cdot 3H_2O$,[10] Nabokoite

Received: April 3, 2014
Published: May 9, 2014

   dx.doi.org/10.1021/ic500793z | *Inorg. Chem.* 2014, 53, 5862–5868

$Cu_7(TeO_4)(SO_4)_5$·KCl,[11] Bairdite $Pb_2Cu_4Te_2O_{10}(OH)_2(SO_4)$-$(H_2O)$,[12] $Cu_7(OH)_6(TeO_3)_2(SO_4)_2$,[13] and Ho_2Cu-$(TeO_3)_2(SO_4)_2$[14] are known. In this work, we have successfully obtained two new tellurite−sulfate compounds of $M_2(TeO_3)$-(SO_4)·H_2O (M = Co, Mn) with quasi-2D layer structure. Herein, we report on their syntheses, structures, and magnetic properties.

EXPERIMENTAL SECTION

Preparation of $Co_2(TeO_3)(SO_4)$·H_2O. Single crystals of $Co_2(TeO_3)(SO_4)$·H_2O were synthesized by a conventional hydrothermal method. A mixture of 3 mmol of $CoSO_4$·$7H_2O$ (3 N, 0.8433 g), 1 mmol of $CoCO_3$·xH_2O (2 N, 0.1189 g), 1.2 mmol of K_2TeO_3 (3 N, 0.3045 g), 0.5 mmol of H_3BO_3 (3 N, 0.0309 g), and 10 mL of deionized water was sealed in an autoclave equipped with a Teflon liner (28 mL). The autoclave was put into a furnace, which was heated at 210 °C for 4 days under autogenous pressure and then cooled to room temperature at a rate of ∼4 °C h^{-1} for 2 days. The fuchsia plated-shaped crystals of $Co_2(TeO_3)(SO_4)$·H_2O were obtained and further dried at 60 °C for 2 h. The powdered samples were prepared by crushing single crystals of $Co_2(TeO_3)(SO_4)$·H_2O, which were used for various physical measurements. The purity of powered samples was confirmed by powder X-ray diffraction (XRD) analysis (Figure S1a in the Supporting Information, SI).

Preparation of $Mn_2(TeO_3)(SO_4)$·H_2O. Single crystals of $Mn_2(TeO_3)(SO_4)$·H_2O were synthesized by a conventional hydrothermal method. A mixture of 1.5 mmol of $MnSO_4$·H_2O (3 N, 0.2535 g), 0.75 mmol of $Ba(OH)_2$·$8H_2O$ (2 N, 0.2366 g), 0.6 mmol of K_2TeO_3 (3 N, 0.1523 g), 0.5 mmol of H_3BO_3 (3 N, 0.0309 g), and 10 mL of deionized water was sealed in an autoclave equipped with a Teflon liner (28 mL). The autoclave was put into a furnace, which was heated at 210 °C for 4 days under autogenous pressure and then cooled to room temperature at a rate of ∼4 °C h^{-1} for 2 days. The white sheetlike crystals of $Mn_2(TeO_3)(SO_4)$·H_2O were obtained and further dried at 60 °C for 2 h. Like $Co_2(TeO_3)(SO_4)$·H_2O, the powdered samples were also prepared by crushing single crystals of $Mn_2(TeO_3)(SO_4)$·H_2O, which were used for similar physical measurements. The purity of powered samples was also confirmed by powder XRD analysis (Figure S1b in the SI).

X-ray Crystallographic Studies. The small crystals of $Co_2(TeO_3)(SO_4)$·H_2O and $Mn_2(TeO_3)(SO_4)$·H_2O (∼0.1 mm × 0.1 mm × 0.05 mm) were selected and mounted on glassy fibers for single-crystal XRD measurements. Data collections were performed on a Rigaku Mercury CCD diffractometer equipped with graphite-monochromated Mo Kα radiation (λ = 0.71073 Å) at 293 K. The data sets were corrected for Lorentz and polarization factors as well as for absorption by a multiscan method.[15] The structure was solved by direct methods and refined by full-matrix least-squares fitting on F^2 by *SHELX-97*.[16] All non-H atoms were refined with anisotropic thermal parameters. The H atoms were located at calculated positions and refined with isotropic thermal parameters. The final refined structural parameters were checked by the *PLATON* program.[17] Crystallographic data and structural refinements are summarized in Table 1. The final refined atomic positions and structural parameters are seen in the Supporting Information (Tables S1−S6).

Magnetic Measurements. Magnetic measurements were performed using a commercial Quantum Design Physical Property Measurement System. Powdered samples of $Co_2(TeO_3)(SO_4)$·H_2O (17.580 mg) and $Mn_2(TeO_3)(SO_4)$·H_2O (60.220 mg) were placed separately in a gel capsule sample holder, which was suspended in a plastic drinking straw. The magnetic susceptibility was measured at 0.1 T from 300 to 2 K (temperature scan of 5 K min^{-1}), and magnetization was measured at 2 K in an applied field from −8 to 8 T (field scan of 0.1 T $step^{-1}$). Moreover, the magnetic susceptibility of $Co_2(TeO_3)(SO_4)$·H_2O was also measured with field-cooling (FC) and zero-field-cooling (ZFC) regimes from 2 to 30 K.

Thermal Analysis. Thermogravimetric analysis (TGA) was performed with a Netzsch STA 449C instrument in a nitrogen atmosphere at a heating rate of 10 °C min^{-1}. The samples were placed in Al_2O_3 crucibles and heated from room temperature to 1000 °C.

Table 1. Crystal Data and Structure Refinement for $M_2(TeO_3)(SO_4)$·H_2O (M = Co, Mn)

formula	$Co_2(TeO_3)(SO_4)$·H_2O	$Mn_2(TeO_3)(SO_4)$·H_2O
fw	407.55	399.57
T, K	room temp	room temp
λ, Å	0.71073	0.71073
space group	*Pbcm*	*Pbcm*
a, Å	7.483(5)	7.661(12)
b, Å	10.181(8)	10.523(18)
c, Å	8.458(6)	8.703(14)
α, deg	90	90
β, deg	90	90
γ, deg	90	90
V, Å^3	644.4(8)	702(2)
Z	4	4
D_{calcd}, g cm^{-3}	4.201	3.783
μ, cm^{-1}	99.16	79.78
GOF on F^2	1.132	1.173
R1, wR2 [$I > 2\sigma(I)$][a]	0.0368, 0.0771	0.0473, 0.1087
R1, wR2 (all data)	0.0398, 0.0785	0.0518, 0.1117

[a] $R1 = \sum||F_o| - |F_c||/\sum|F_o|$; $wR2 = \{\sum w[(F_o)^2 - (F_c)^2]^2/\sum w[(F_o)^2]^2\}^{1/2}$.

RESULTS AND DISCUSSION

Structural Descriptions. X-ray analysis indicates clearly that the compounds of $M_2(TeO_3)(SO_4)$·H_2O (M = Co, Mn) are isostructural and crystallize in the orthorhombic system of space group *Pbcm* with a = 7.483(5) Å, b = 10.181(8) Å, c = 8.458(6) Å and a = 7.661(12) Å, b = 10.523(18) Å, c = 8.703(14) Å, respectively. Because they are isostructural, $Co_2(TeO_3)(SO_4)$·H_2O is selected as a representative for the detailed description of their structures. For $Co_2(TeO_3)(SO_4)$·H_2O, there is one Co atom, one Te atom, and one S atom in an asymmetric unit, in which the Co atom locates on the Wyckoff position of 8e and the Te and S atoms are both in the position of 4d. As shown in Figure 1, all of Co^{2+} ions are equivalent and are coordinated by six O atoms, forming CoO_6 octahedra. All of CoO_6 octahedra are distorted, with Co−O bond lengths ranging from 2.062(4) to 2.229(4) Å and O−Co−O bond angles of the CoO_6 octahedron ranging from 73.4(2)° to 174.55(14)°. Each CoO_6 octahedron is surrounded by three Te atoms, two S atoms, and three Co atoms, in which Co connects to Te and S with corner-sharing O atoms [(O5, O1) and (O3, O6), respectively], while the Co atoms connect to each other with two edge-sharing (O5···O5 and O1···O3) and one corner-sharing (O4). Both S and Te atoms have independent crystallographic sites. S atoms are tetrahedrally coordinated by four O atoms, forming a nearly regular SO_4^{2-} tetrahedron, with S−O distances ranging from 1.473(7) to 1.503(6) Å [averaging at 1.483(6) Å] and O−S−O angles in the range of 107.6(4)−110.6(4)°, giving its mean value of 109.4(1)°, which is close to the ideal tetrahedral angle, 109.5°. This feature of the SO_4^{2-} tetrahedron is very common in sulfates. It is noted that all of the Te atoms are coordinated by three O atoms, forming a quite distorted TeO_3 trigonal pyramid with lone-pair $5S^2$ in Te^{4+} ions. The Te−O distances are close to 1.9 Å, and the angles of O−Te−O are from 95.7(3)° to 98.75(19)°. Each O atom in the TeO_3 trigonal pyramid connects with two Co ions by corner-sharing, so all of TeO_3 trigonal pyramids are

dx.doi.org/10.1021/ic500793z | Inorg. Chem. 2014, 53, 5862−5868

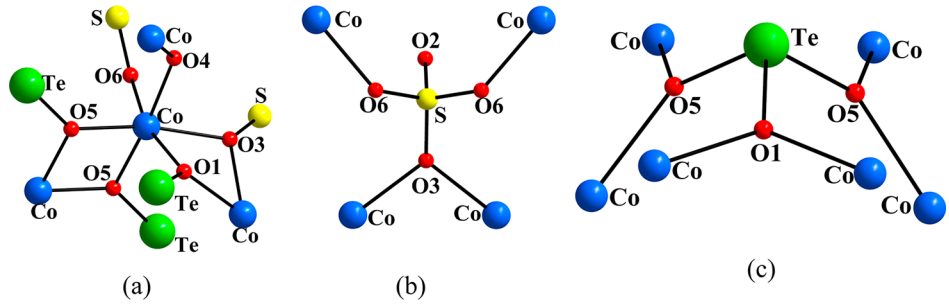

Figure 1. Views of the oxygen-coordination environments for (a) Co, (b) S, and (c) Te atoms in $Co_2(TeO_3)(SO_4)\cdot H_2O$.

surrounded by six Co ions. The bond valence sum (BVS) calculations of Co, S, and Te are 1.931, 5.858, and 4.075, respectively, confirming that these atoms are very close to their postulated oxidation states. Besides, according to the results of the BVS, the value of O4 is 0.627, which shows that it should be connected to double H atoms, forming a water (H_2O) molecule for charge balancing the formula.

The linkage of polyhedra is shown in Figure 2. CoO_6 octahedra are connected to each other through edge-sharing (O5···O5 and O1···O3) to form a skew chain $[CoO_6]_\infty$ running along the *c* axis (Figure 2a). The skew chains are further connected via corner-sharing oxygen (O4), forming a twisted 2D layer in the *bc* plane (Figure 2b). Such a linkage of chains shows tunnel networks running along the *a* axis, in which a distorted TeO_3 trigonal pyramid is located (Figure 2c). It is noted that the linkage of CoO_6 octahedra in $Co_2(TeO_3)(SO_4)\cdot H_2O$ is quite similar to that of NiO_6 octahedra in $Ni_3(MoO_4)(TeO_3)_2$.[18] Moreover, the neighboring Co···Co separations in the chains are 3.1542(19) and 3.2937(26) Å, showing that the skew chains are not uniform but alternative, while the shortest interchain Co···Co separation is 3.7532(27) Å. The three-dimensional (3D) framework of $Co_2(TeO_3)(SO_4)\cdot H_2O$ is shown in Figure 3. A typical layer structure can be seen in the *ac* plane, in which the layers built by Co chains and a distorted TeO_3 trigonal pyramid are running along the *a* axis and are separated by SO_4^{2-} tetrahedra (Figure 3a). It is noted that the layers are corrugated, showing a wavelike feature in the *ab* plane (Figure 3b). The twisted angle in the layer is about 118.89(7)°, and the shortest Co···Co separation between layers is 5.145(3) Å.

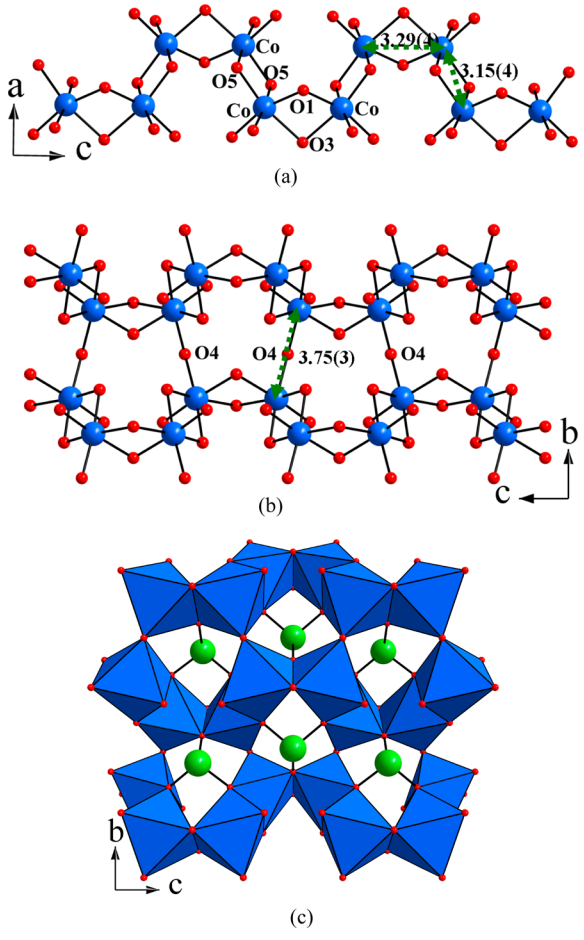

Figure 2. Views of the linkage of polyhedra for (a) the intrachain running along the *c* axis, (b) interchains in the *bc* plane, and (c) a distorted honeycomb layer with TeO_3 groups. The distances (Å) of neighboring Co−Co for intrachains and interchains are noted.

Because H_2O, TeO_3^{2-}, and SO_4^{2-} groups are nonmagnetic, the spin−lattices in $Co_2(TeO_3)(SO_4)\cdot H_2O$ are determined by the topological arrangements of magnetic Co^{2+} ions. When H_2O, TeO_3^{2-}, and SO_4^{2-} groups are removed from the structure of $Co_2(TeO_3)(SO_4)\cdot H_2O$, magnetic Co^{2+} ions are found to form a distorted honeycomb spin−lattice in the layers, as shown in Figure 4. The distances of the neighboring Co···Co in the honeycomb lattice are 3.1542(19), 3.2937(26), and 3.7532(27) Å, respectively, which correspond to the nearest separations of Co···Co in the chains and between the chains, while the angles of Co···Co···Co in the honeycomb lattice are 104.4(3)°, 107.2(5)°, and 111.9(1)°.

MAGNETIC PROPERTIES

$Co_2(TeO_3)(SO_4)\cdot H_2O$. Figure 5 shows the temperature dependencies of the magnetic susceptibility (χ) and the corresponding reciprocal (χ^{-1}) of $Co_2(TeO_3)(SO_4)\cdot H_2O$. The susceptibility increases with decreasing temperature, while a rapid upturn is observed below 15 K, showing the onset of magnetic ordering. A typical Curie−Weiss behavior is observed above 30 K, giving the Curie constant C = 6.587(6) emu mol^{-1} K and the Weiss temperature θ = −32.4(1) K. The effective magnetic moment of Co^{2+} ions in the system is calculated to be 5.13(3) μ_B using the equation of $\mu_{eff}^2 = 8C$, which is larger than the theoretical spin value of 3.873 μ_B for Co^{2+} ions ($S = {}^3/_2$; $g = 2$) obtained by $\mu_{eff}^2 = gS(S+1)$, indicating a large orbital moment contribution of Co^{2+} in the oxygen octahedral environment.[19,20] This characteristic feature of Co^{2+} ions can also be found in many CoO-based oxides such as $BaCo_2V_2O_8$,[21] $BiCo_2BP_2O_{10}$,[22] and CoV_2O_6.[23] Also, the negative Weiss temperature indicates that the dominative interactions between magnetic Co^{2+} ions are antiferromagnetic

dx.doi.org/10.1021/ic500793z | Inorg. Chem. 2014, 53, 5862−5868

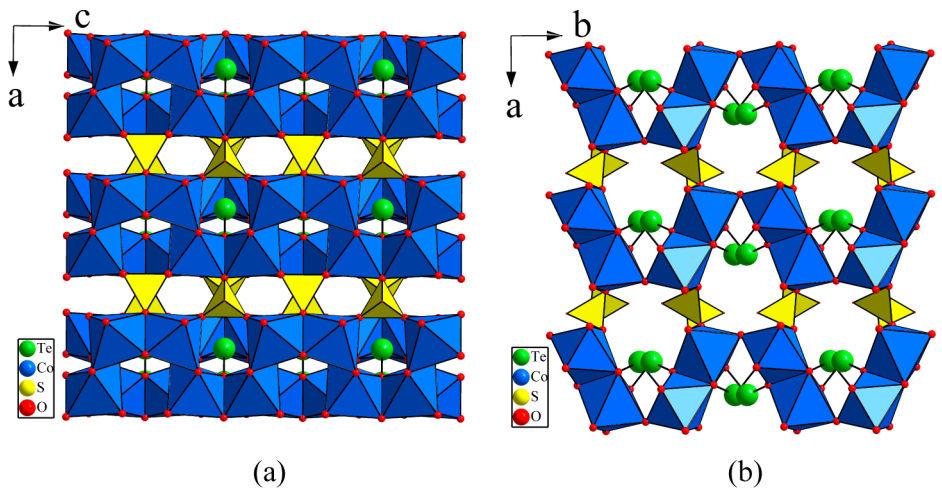

Figure 3. Views of the layer structure of $Co_2(TeO_3)(SO_4)\cdot H_2O$ on (a) the *ac* plane and (b) the *ab* plane.

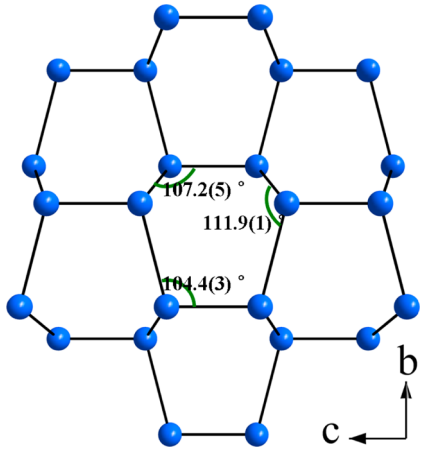

Figure 4. Spin−lattice with a distorted honeycomb network built by magnetic Co^{2+} ions in the *bc* plane.

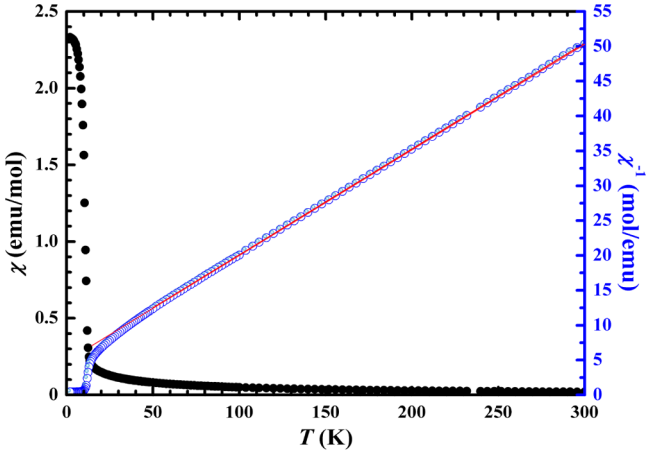

Figure 5. Temperature dependence of the magnetic susceptibility and the corresponding reciprocal for $Co_2(TeO_3)(SO_4)\cdot H_2O$.

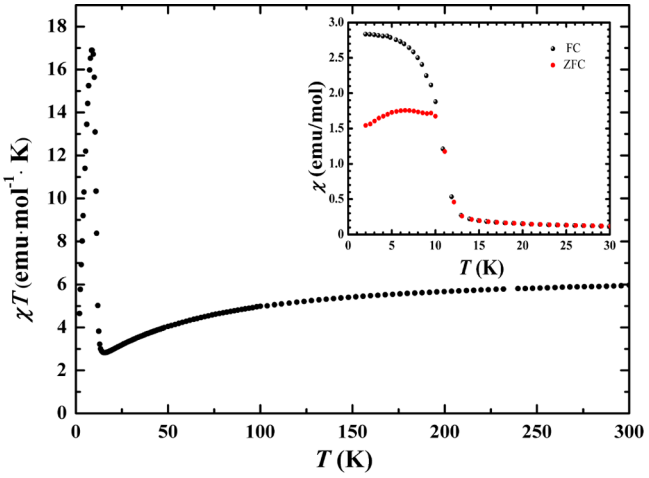

Figure 6. Variation of χT with the temperature for $Co_2(TeO_3)(SO_4)\cdot H_2O$. The inset shows the susceptibility measured with the FC and ZFC regimes.

in nature. Figure 6 shows the plot of χT versus temperature (T). The value of χT is ~5.9 emu mol^{-1} K at 300 K and then reaches its minimum of 2.8 emu mol^{-1} K at ca. 14.7 K with decreasing temperature, while the maximum of 14.9 emu mol^{-1} K is obtained at 8.8 K, indicating the appearance of a ferromagnetic correlation. To further identify such a ferromagnetic correlation, low-temperature magnetic susceptibility of $Co_2(TeO_3)(SO_4)\cdot H_2O$ is measured at the ZFC and FC regimes (the inset of Figure 6). A clear history is seen below 10 K between the ZFC and FC regimes, confirming the characteristic irreversibility of a weak ferromagnetic component. Considering a negative Weiss temperature, such a weak ferromagnetic component may originate from spin-canted or ferrimagnetic behaviors. However, the ferromagnetic moment is roughly estimated to be ~0.20(9) μ_B/Co^{2+} in a field of 1000 Oe, which corresponds to 6.9(7)% of the full Co^{2+} ion (3 μ_B) moment, suggesting that the system is a canted antiferromagnet.

Figure 7 shows isothermal magnetization as a function of the applied field ($M-H$) at 2 K. The magnetization rapidly increases in the low-field region, while clear hysteresis and remnant magnetization are observed near H = 0, evidencing a ferromagnetic component in the system. The linear behavior of the magnetization is seen above H of 3000 Oe, and no magnetization saturation is seen up to 8 T. These behaviors are also characteristic features of a canted antiferromagnet, which are in good agreement with the susceptibility data. In addition, the weak ferromagnetic moment (M_{WF}) of ~0.2 μ_B can be obtained by subtracting the linear component ($M_{WF} = M -$

dx.doi.org/10.1021/ic500793z | Inorg. Chem. 2014, 53, 5862−5868

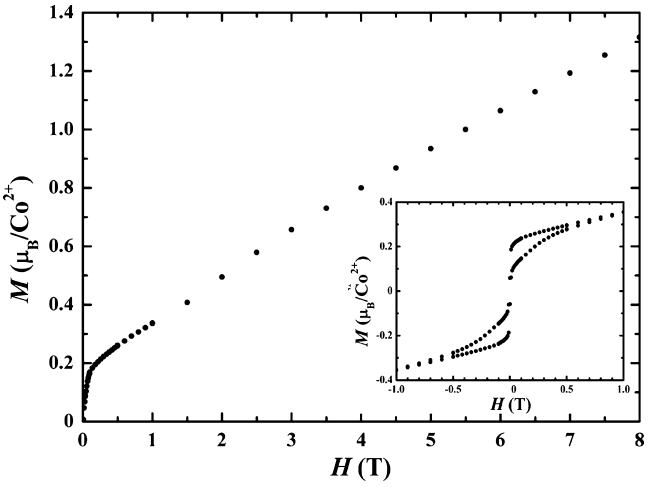

Figure 7. Curve of magnetization versus applied field at 2 K for $Co_2(TeO_3)(SO_4)\cdot H_2O$. The inset shows an enlarged view of the low-field range.

χH) from the magnetization, and the canted angle θ of 3.82° can be estimated on the basis of the definition of $M_{WF} = M_F \sin \theta$ by assuming the full moment (M_F) of 3 μ_B for Co^{2+} ions with $S = {}^3/_2$.[24]

$Mn_2(TeO_3)(SO_4)\cdot H_2O$. Figure 8 shows the temperature dependencies of the magnetic susceptibility (χ) and the

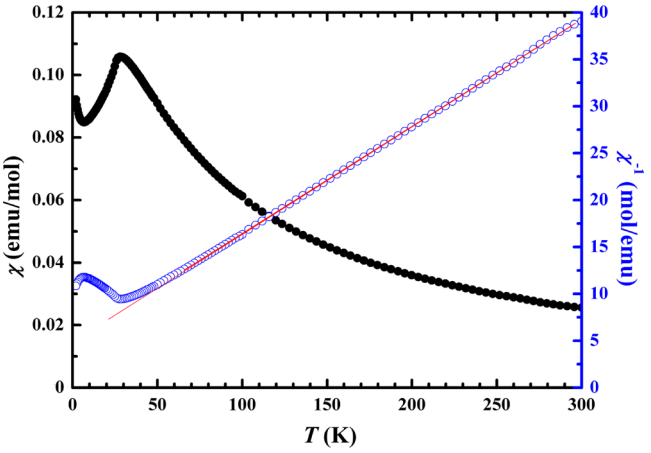

Figure 8. Temperature dependencies of the magnetic susceptibility and the corresponding reciprocal for $Mn_2(TeO_3)(SO_4)\cdot H_2O$.

corresponding reciprocal (χ^{-1}) of $Mn_2(TeO_3)(SO_4)\cdot H_2O$. The magnetic susceptibility increases with decreasing temperature, while a peak is observed at ~28 K, indicating the onset of antiferromagnetic ordering. A typical Curie–Weiss behavior is observed above 50 K, giving the Curie constant C = 8.755(8) emu mol^{-1} K and the Weiss temperature θ = −43.8(4) K. The effective magnetic moment of Mn^{2+} ions in the system is calculated to be 5.918(1) μ_B, which is quite close to the theoretical spin value of 5.916(1) μ_B for Mn^{2+} ions ($S = {}^5/_2$; g = 2), showing Mn^{2+} ions of $Mn_2(TeO_3)(SO_4)\cdot H_2O$ with a high-spin state. Also, the negative Weiss temperature indicates that the dominative interactions between magnetic Mn^{2+} ions are antiferromagnetic. Figure 9 shows the plot of χT versus temperature (T). The value of χT is ~7.7 emu mol^{-1} K at 300 K and keeps on falling with decreasing temperature, supporting the dominative antiferromagnetic interaction exchanges in the

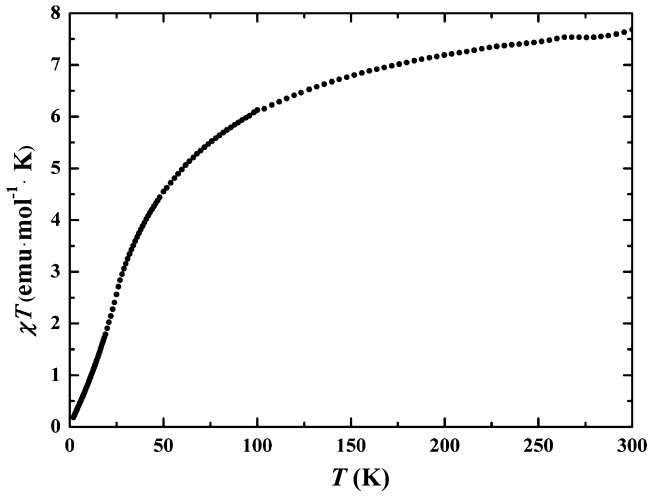

Figure 9. Variation of χT with the temperature for $Mn_2(TeO_3)(SO_4)\cdot H_2O$.

system. Unlike that observed in $Co_2(TeO_3)(SO_4)\cdot H_2O$, there are not any rapid upturns in the plot of χT–T, ruling out the appearance of a ferromagnetic component. Figure 10 shows

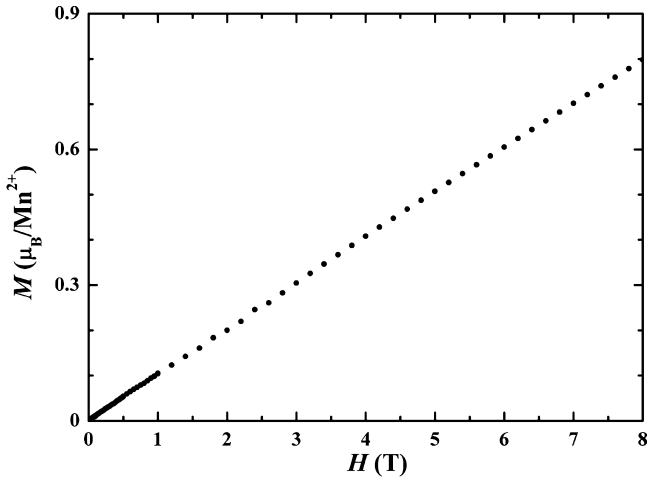

Figure 10. Curve of magnetization versus applied field at 2 K for $Mn_2(TeO_3)(SO_4)\cdot H_2O$.

isothermal magnetization as a function of the applied field (M–H) at 2 K. The magnetization shows an increase in the nearly linear manner and does not saturate even in 8 T. Furthermore, no hysteresis and remnant magnetization are observed. These features are also consistent with antiferromagnetic ordering below 28 K for $Mn_2(TeO_3)(SO_4)\cdot H_2O$.

It is quite interesting to make a comparison of the magnetic behaviors between isostructural $M_2(TeO_3)(SO_4)\cdot H_2O$ (M = Co, Mn). We note that both compounds exhibit similar antiferromagnetic exchange couplings because of the fact that magnetic ions (Co^{2+} or Mn^{2+}) have similar spin–lattices with a distorted honeycomb feature. $Co_2(TeO_3)(SO_4)\cdot H_2O$ shows a magnetic transition at the Néel temperature of ~15 K with the Weiss temperature θ = −32.4(1) K, while $Mn_2(TeO_3)(SO_4)\cdot H_2O$ exhibits that at the Néel temperature of ~28 K with Weiss constant θ = −43.8(4) K. These differences may indicate that different magnitudes of antiferromagnetic interactions between magnetic ions, in which a large interaction between Mn^{2+} ions arises from a large spin number of Mn^{2+} ions with $S = {}^5/_2$ in the

dx.doi.org/10.1021/ic500793z | Inorg. Chem. 2014, 53, 5862–5868

similar distorted honeycomb lattice. This finding is also seen in isostructural $BiM_2BP_2O_{10}$ (M = Co, Ni) with different spin number S in a similar spin−lattice.[22] In addition, Mn^{2+} ions ($3d^5$, $t_{2g}^3e_g^2$) usually show a typical Heisenberg-like feature with small spin−orbit coupling due to the complete quenching of the orbital degrees of freedom in the octahedral ligand field, while Co^{2+} ions ($3d^7$, $t_{2g}^5e_g^2$) show a large spin−orbit coupling with an Ising-like feature due to the t_{2g} orbital degrees of freedom and contribution of large orbital angular momentum in the octahedral ligand field. Therefore, it is well understood that $Mn_2(TeO_3)(SO_4)\cdot H_2O$ exhibits a typical spin-collinear antiferromagnetic ground state, while $Co_2(TeO_3)(SO_4)\cdot H_2O$ displays a spin-nonlinear canted antiferromagnetic ground state at low temperature, although they have similar crystal structures with a centrosymmetric space group of *Pbcm*. Such spin-canted behaviors can also be found in many Co-based compounds with a centrosymmetric space group.[25−27] This may be due to a nonzero correlation of the Dzyaloshinskii−Moriya interactions[28,29] in centrosymmetric magnetic materials, as seen in spin-canting behaviors of β-$CrAsO_4$ with the $ZnSO_4$-type structure.[30]

Thermal Analysis. To investigate the thermal stability of $M_2(TeO_3)(SO_4)\cdot H_2O$ (M = Co, Mn), the samples are heated up to 1000 °C under a nitrogen atmosphere in Figure 11. It is noted that both compounds are stable with increasing temperature up to 265 °C, while the onset of weight loss is clearly observed. Although slightly different thermal stabilities can be found in these isostructural compounds, a quite similar behavior of the weight loss is seen with two main steps including a plateau and a rapid drop. For $Co_2(TeO_3)(SO_4)\cdot H_2O$, the loss in the weight of the sample starts above 265 °C, while a plateau is seen in the temperature range of 510−710 °C. This step may be attributed to the loss of H_2O molecules because the observed weight loss of 4.4% for the plateau is close to the calculated one of H_2O in $Co_2(TeO_3)(SO_4)\cdot H_2O$, 4.3%. Further, a rapid drop in the weight loss curve is clearly seen above 710 °C, indicating decomposition of the system with the release of SO_3 and TeO_2. The total weight loss is about 25.6% at 1000 °C. For $Mn_2(TeO_3)(SO_4)\cdot H_2O$, the loss in the weight of the sample also starts above 265 °C, while a plateau corresponding to the weight loss of ∼4.4% is seen in the temperature range of 460−800 °C. This shows that the first step is the loss of H_2O molecules in the system, which is similar to that of $Co_2(TeO_3)(SO_4)\cdot H_2O$. Further, decomposition of the system with the release of SO_3 and TeO_2 is suggested on the basis of a rapid drop in the weight loss curve above 810 °C. At 1000 °C, the total weight loss reaches ∼24.0%. It must be noted that the final residuals of thermal analysis are not further characterized because of the fact that the residuals have been melted with the TGA bucket made of Al_2O_3 under such high temperature.

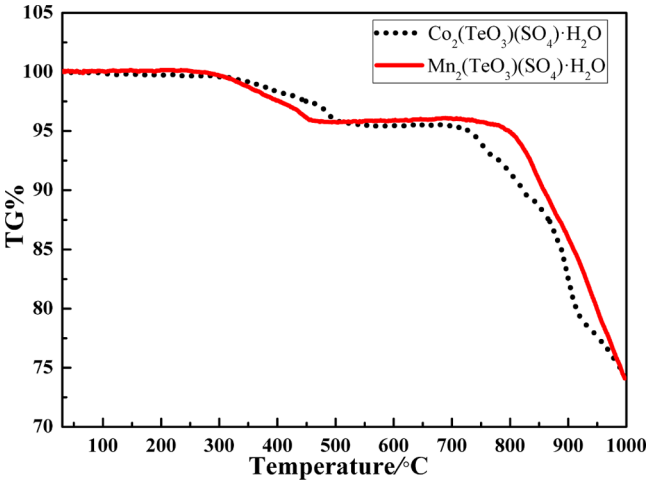

Figure 11. TGA curves of $M_2(TeO_3)(SO_4)\cdot H_2O$ (M = Co, Mn).

CONCLUSION

We have successfully obtained new tellurite−sulfate compounds $M_2(TeO_3)(SO_4)\cdot H_2O$ (M = Co, Mn) by a hydrothermal method. The titled compounds are found to crystallize in the orthorhombic system of space group *Pbcm*, which displays a layer structure with a wavelike feature in the *ab* plane. Two isostructural compounds can be stable at room temperature, while the loss of H_2O molecules happens with heating above ∼265 °C. Also, upon removal of nonmagnetic ions from the structures of the titled compounds, magnetic Co^{2+} or Mn^{2+} ions were found to be arranged in a distorted honeycomb-like spin−lattice in the layers. Magnetic measurements confirmed that $Co_2(TeO_3)(SO_4)\cdot H_2O$ exhibits a canted antiferromagnetic ordering, while $Mn_2(TeO_3)(SO_4)\cdot H_2O$ exhibits a typical 3D collinear antiferromagnetic ground state. The different magnetic behaviors are suggested to arise mainly from magnetic ions with different spin numbers themselves in the octahedral ligand field.

ASSOCIATED CONTENT

Supporting Information

Final refined atomic positions and structural parameters and simulated and experimental powder XRD patterns for $Co_2(TeO_3)(SO_4)\cdot H_2O$ and $Mn_2(TeO_3)(SO_4)\cdot H_2O$. This material is available free of charge via the Internet at http://pubs.acs.org.

AUTHOR INFORMATION

Corresponding Author

*E-mail: hezz@fjirsm.ac.cn or hcz1988@hotmail.com.

Notes

The authors declare no competing financial interest.

ACKNOWLEDGMENTS

This work was financially supported by the National Basic Research Program of China (Grant 2012CB921701).

REFERENCES

(1) Kodama, K.; Masashi, T.; Horvatic, M.; Berthier, C.; Kageyama, H.; Ueda, Y.; Miyahara, S.; Becca, F.; Mila, F. *Science* **2002**, *298*, 395−399.

(2) Sebastian, S. E.; Harrison, N.; Batista, C. D.; Balicas, L.; Jaime, M.; Sharma, P. A.; Kawashima, N.; Fisher, I. R. *Nature* **2006**, *441*, 617−620.

(3) Bartlett, B. M.; Nocera, D. G. *J. Am. Chem. Soc.* **2005**, *127*, 8985−8993.

(4) Smirnova, O.; Azuma, M.; Kumada, N.; Kusano, Y.; Matsuda, M.; Shimakawa, Y.; Takei, T.; Yonesaki, Y.; Kinomura, N. *J. Am. Chem. Soc.* **2009**, *131*, 8313−8317.

(5) Smith, R. W.; Keszler, D. A. *J. Solid State Chem.* **1991**, *93*, 430−435.

(6) Tsukada, I.; Sasago, Y.; Uchinokura, K. *Phys. Rev. B* **1999**, *60*, 6601−6607.

(7) Belik, A. A.; Azuma, M.; Matsuo, A.; Whangbo, M.-H.; Koo, H.-J.; Kikuchi, J.; Kaji, T.; Okubo, S.; Ohta, H.; Kindo, K.; Takano, M. *Inorg. Chem.* **2005**, *44*, 6632−6640.
(8) Vogt, R.; Mueller Buschbaum, H. *Z. Anorg. Allg. Chem.* **1990**, *591*, 167−173.
(9) Gou, W. B.; He, Z. Z.; Yang, M.; Zhang, W. L.; Cheng, W. D. *Inorg. Chem.* **2013**, *52*, 2492−2496.
(10) Frost, R. L.; Keeffe, E. C. *J. Raman Spectrosc.* **2008**, *39*, 1794−1798.
(11) Pertlik, F.; Zemann, J. *Mineral. Petrol.* **1988**, *38*, 291−298.
(12) Kampf, A. R.; Mills, S. J.; Housley, R. M.; Rossman, G. R.; Marty, J.; Thorne, B. *Am. Mineral.* **2013**, *98*, 1315−1321.
(13) Pertlik, F.; Zemann, J. *Monatsh. Chem.* **1988**, *119*, 311−317.
(14) Lin, J.; Diefenbach, K.; Cross, J. N.; Babo, J.-M.; Albrecht-Schmitt, T. E. *Inorg. Chem.* **2013**, *52*, 13278−13281.
(15) *CrystalClear*, version 1.3.5; Rigaku Corp.: The Woodlands, TX, 1999.
(16) Sheldrick, G. M. *Crystallographic Software Package, SHELXTL*, version 5.1; Bruker AXS: Madison, WI, 1998.
(17) Spek, A. L. *J. Appl. Crystallogr.* **2003**, *36*, 7.
(18) Zhang, S. Y.; Jiang, H. L.; Sun, C. F.; Mao, J. G. *Inorg. Chem.* **2009**, *48*, 11809−11820.
(19) Mabbs, F. E.; Machin, D. J. *Magnetism and Transition Metal Complexes*; Chapman and Hall: London, 1973.
(20) Figgis, B. N.; Hitchman, M. A. *Ligand Field Theory and Its Applications*; Wiley-VCH: New York, 2000.
(21) He, Z.; Fu, D.; Kyômen, T.; Taniyama, T.; Itoh, M. *Chem. Mater.* **2005**, *17*, 2924−2926.
(22) Zhang, W. L.; He, Z. Z.; Xia, T. L.; Luo, Z. Z.; Zhang, H.; Lin, C. S.; Cheng, W. D. *Inorg. Chem.* **2012**, *51*, 8842−8847.
(23) He, Z.; Yamaura, J.; Ueda, Y.; Cheng, W. *J. Am. Chem. Soc.* **2009**, *131*, 7554−7555.
(24) He, Z.; Ueda, Y.; Itoh, M. *J. Solid State Chem.* **2007**, *180*, 1770−1774.
(25) Yang, T.; Lin, J. H. *J. Solid State Chem.* **2013**, *198*, 1−5.
(26) Alexandre, M.-R.; Daniel, J. P. *Polyhedron* **2013**, *52*, 650−657.
(27) Cheng, X. N.; Xue, W.; Huang, J. H.; Chen, X. M. *Dalton Trans.* **2009**, *29*, 5701−5707.
(28) Dzyaloshinskii, I. *Sov. Phys. JETP* **1957**, *5*, 1259−1272.
(29) Moriya, T. *Phys. Rev.* **1960**, *120*, 91−98.
(30) Attfield, J. P.; Cheetham, A. K.; Johnson, D. C.; Torardi, C. C. *Inorg. Chem.* **1987**, *26*, 3379−3383.